A reprint from

OPTICAL ENGINEERING

ISSN 0091-3286

Multiresolution analysis of two-dimensional 1/*f* processes: approximation methods for random variable transformations

John J. Heine
University of South Florida
Department of Radiology
Digital Medical Imaging Program
Tampa, Florida 33612-4799
E-mail: heine@splinter.moffitt.usf.edu

Stanley R. Deans, MEMBER SPIE
University of South Florida
Department of Physics
Tampa, Florida 33620-5700
E-mail: deans@splinter.moffitt.rad.usf.edu

Deepak Gangadharan
Laurence P. Clarke, MEMBER SPIE
University of South Florida
Department of Radiology
Digital Medical Imaging Program
Tampa, Florida 33612-4799
E-mail: clarke@splinter.moffitt.usf.edu

Abstract. The multiresolution wavelet expansion is used as a simplifying mechanism for the parametric analysis of complicated highly correlated random fields. A previously developed approximation method is applied to simulated statistically self-similar random fields for further evaluation. This approach can be considered as a simplifying method for random variable transformations for some important applications. The approach overcomes many of the difficulties associated with predicting the output field probability distribution function resulting from passing a non-Gaussian random process through a linear network. Here, the multiresolution wavelet expansion can be considered as a linear network. The ideas are illustrated with three related simulated noise fields: a white noise input field distributed proportional to a zero order hyperbolic Bessel function and two 1/*f* noise processes resulting from filtering the white noise process. The fields are analyzed with an orthogonal multiresolution wavelet expansion. The expansion components are studied with parametric analysis, where the probability models are all derived from one family of functions. In addition, the study illustrates some interesting non-intuitive statistical properties of the filtered fields. [S0091-3286(99)01809-7]

Subject terms: multiresolution; wavelet transformation; parametric statistics; random variables; self-similarity.

Paper 980021 received Jan. 21, 1998; revised manuscript received Oct. 28, 1998; accepted for publication Apr. 15, 1999.

1 Introduction

This work is an outgrowth of previous multiresolution statistical analysis applied to digital mammography[1–4] (DM). The current thrust of our mammography work is to develop a firm grasp of the statistical properties of normal tissue with the goal of developing reliable automated methods for the detection of clinically normal images. This is an important application in DM when considering (1) the majority of signal from a given image arises from normal tissue, even when abnormalities are present, and (2) the vast majority of mammograms are clinically normal, roughly 90%. Often, mammograms have irregular multimodal gray scale histograms and can be considered as highly correlated random fields that are considered too irregular or complicated for parametric analysis. However, by reasonable approximations, we have evidence indicating this assumption may not always be correct. A growing body of work indicates that mammograms, to some degree, can be considered as statistically self-similar processes.[4–7] The term self-similarity often implies fractal behavior. The work presented here is a theoretical study of synthetic imagery generated from a statistical understanding of mammograms with the intent of gaining a better understanding of the irregularities common to mammograms and verifying initial findings.[1–4]

Fractal methods have become a popular analysis tool used for characterizing image textures. The analysis usually involves estimating the fractal dimension based on measuring some scale invariant property. Fractal applications include the analysis of natural scenes, such as earth topography, trees, foliage, clouds, and astronomy data,[8–13] the study of radiographs for tissue and bone classification,[4–7,14] and image compression.[15] Similarly, fractal methods can be used in detection problems such as finding man made objects imbedded in natural backgrounds or edges. Often these anomalies cause abrupt changes in the fractal characterization.[11,16]

Natural scene images consisting of various surfaces and patterns often share a common property in that the associated power spectra have similar behavior.[9,13] That is, the 2-D power spectra drops off roughly as $1/f^{2\beta}$, where β is a positive parameter related to the fractal dimension. Noise with this power spectrum form is often referred to as a 1/*f* process, or 1/*f* noise, and is related to fractional Brownian motion[17] under certain conditions. For this study, we use β as the parameter of interest to avoid confusion, rather than the fractal dimension; the corresponding relationships with the fractal processes and Brownian surfaces can be found elsewhere.[8,18] Qualitatively, larger β implies more image irregularity. There is evidence[9,13] for many natural scene images $\beta \approx 1$. This implies that the power is roughly distributed evenly across the spectrum when viewed on a $\log_2$ scale (octave splitting). For mammograms in our database $\beta \approx 1.5$, implying more irregularity. There are many methods for measuring the fractal behavior of a given image in addition to the power spectrum analysis, and the connection among the various methods is not always clear. Several methods and relationships are discussed elsewhere.[10,11,19–21]

2 Current Study

In this paper, we present a multiresolution analysis of simulated 2-D 1/f processes. The noise fields are generated by driving stationary white noise, with a given parametric probability distribution, through a linear filtering operation, where the simulation input field statistical properties and filter functional form are based on the analysis of high resolution mammograms.[4] The intriguing aspect of the study is that a stationary stochastic process is used as the input to a linear filtering operation, and the output can be very irregular with a multimodal gray value histogram for certain values of β. The basic idea is to generate random fields that behave similar to that of mammograms and study the corresponding multiresolution statistical properties. We found that for certain bandlimited detection problems in DM, the analysis of the wavelet expansion components can be used as a simplifying mechanism. This approach is based on analyzing the individual expansion components with simple parametric approximations rather than the analysis of the raw field. The work presented here is further demonstration of this idea and can be considered as making inroads into the more general problem: Determining the output field probability density function (pdf) given a non-Gaussian distributed random field as the input to a linear network. For many cases, this problem is not trivial and cannot be solved in closed form using standard random variable (RV) transformation techniques. For instance, if we generate a new RV by forming linear combinations of other RVs, with different weighting coefficients, the corresponding new pdf might be found providing that (a) the original distribution parametric form is known; (b) in the general case, there are not too many variates in the transform but less than enough to use central limit theorem arguments; and (c) the variates are uncorrelated and statistically independent. When we consider the many operations involved with the wavelet analysis, this problem is for all practical purposes too hard to track for all but Gaussian input fields, although there are some cases where prediction is possible. If the input is a wideband process, or has a frequency spectrum much wider than the network bandwidth, the output field will be approximately Gaussian distributed.[22] This applies regardless of input field pdf.

3 The 1/f Processes and Multiresolution Analysis

3.1 *1/f Generation*

Fourier domain filtering is used to generate the simulations

$$S_0(f)=H(f)S(f) \quad \text{with } f=(f_x,f_y), \tag{1}$$

where (f_x,f_y) are two dimensional Cartesian frequency domain coordinates. The inverse Fourier transform (FT) of $S(f)$, is the simulation input field, $s(x,y)$, and is a white noise process distributed proportional to a modified hyperbolic Bessel function,[23] $p(z)=k\pi^{-1}k_0(k|z|)$, where z is an arbitrary gray value located at some arbitrary spatial location (x,y), k is a constant, $S_0(f)$ is the FT of the output, or simulation, process denoted by $s_0(x,y)$, and $H(f)$ is the frequency domain transfer function with inverse FT $h(x,y)$, the impulse response function. Here we use capitals to indicate the Fourier domain. The $s(x,y)$ simulation method is discussed in Section 4. Explicitly, $H(f)$ is given by

$$H(f_x,f_y)=(f_x^2+f_y^2)^{-\beta/2}. \tag{2}$$

Three simulations are generated and analyzed with multiresolution method: case 1, the white noise process, $s(x,y)$, defined in Eq. (1) and used as the input for the 1/f simulations; and cases 2 and 3, two 1/f simulations that correspond to $\beta=1.0$ and $\beta=1.5$ in Eq. (2), respectively. The latter case is modeled after the previous mammography studies and shows irregular behavior. The fields are 2048 $\times$2048 pixels with 16-bit accuracy.

We have used the model in Eq. (1) with Eq. (2) to analyze mammograms,[4] where $s(x,y)$ is the unknown; this is discussed further in Section 4. This development, of substituting Eq. (2) into Eq. (1), can be taken as the 2-D generalization of an earlier approach[24] used to analyze flicker noise based on considering fractional order integration. Wornell[17] provides a detailed discussion of this earlier work and how it relates to Brownian motion and fractional calculus. A thorough treatment of fractional calculus is given by Oldham and Spanier.[25] We present one possible 2-D generalization of this earlier work in the Appendix. Rather than just plow through Eq. (1), it is instructive to explore the functional form of $h(x,y)$, and work the operation starting from the image domain in contrast to starting in the Fourier domain. As demonstrated in the Appendix, this alternative approach provides insight into the irregular statistical properties often associated with mammograms that is not apparent in Eqs. (1) and (2).

3.2 *Multiresolution Wavelet Expansion*

Briefly, the multiresolution image expansion takes the form of a sum of images given by the identity[26]

$$f_0=(f_0-f_1)+(f_1-f_2)+(f_2-f_3)+\cdots+(f_{J-1}-f_J)+f_J, \tag{3}$$

where the f_1 image is the next coarser representation of f_0 and f_2 is the next coarser approximation of f_1 and so on. The image that contains the *difference* information between the successive f_j images $(f_{j-1}-f_j)$ is designated by d_j, thus

$$f_0=d_1+d_2+d_3+\cdots+d_J+f_J. \tag{4}$$

The d_j images, referred to as the detail images, are not correlated in the sense that $\langle d_j d_k\rangle=0$ for $j\neq k$, and are the components of interest in this study. Smaller j indicates finer detail and f_j is a low resolution version of the raw field. The wavelet analysis is performed with two dimensional separable convolutions using the symmlet basis with 12 coefficients,[27] where down sampling is applied in the

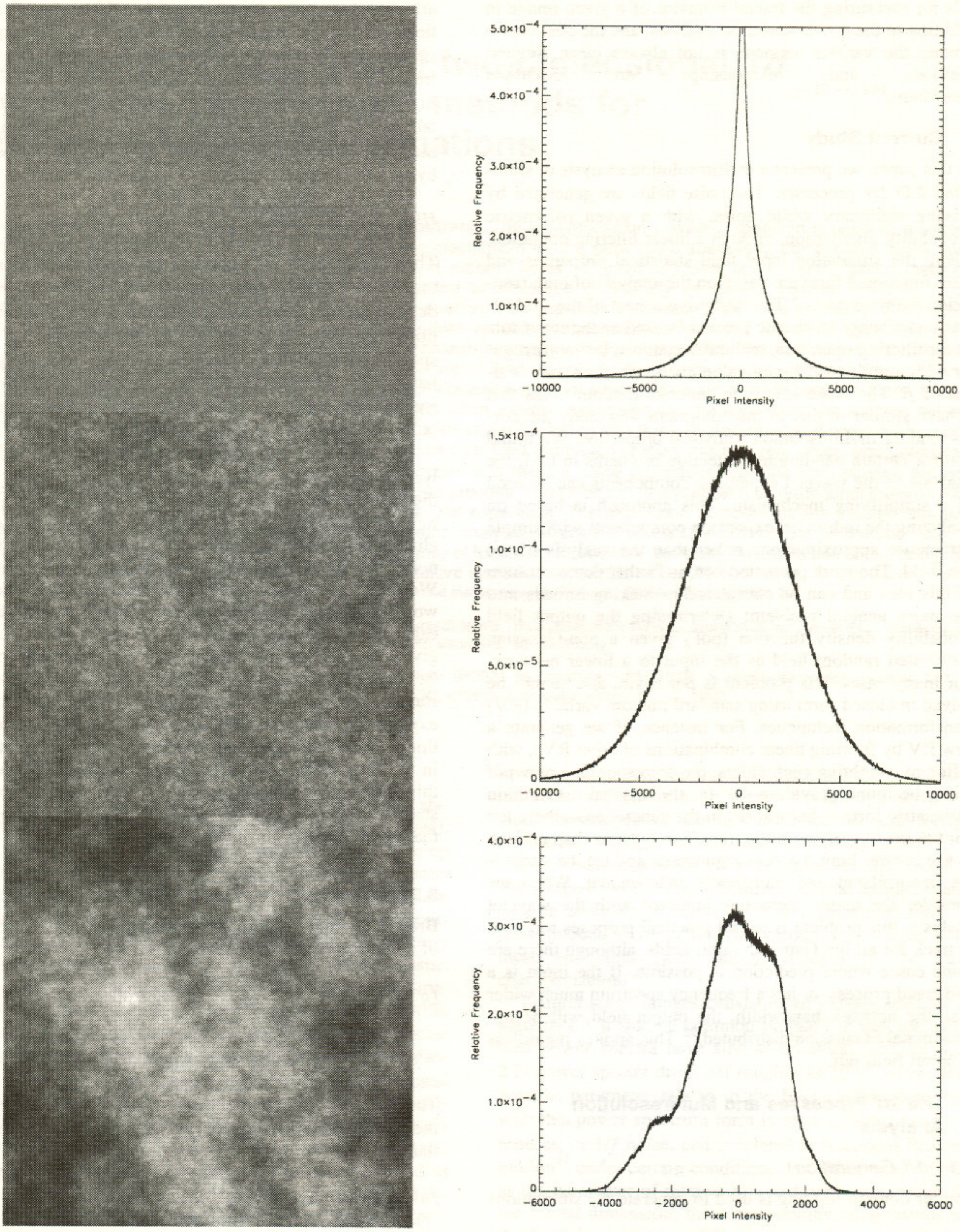

Fig. 1 2048×2048 simulations and associated histograms for the three cases: (a) case 1 (top), the raw k_0 distributed field; (b) case 2, the raw field filtered with a 1/*f* filter; and (c) case 3, the raw field filtered with a $1/f^{1.5}$ filter. Note that somewhat irregular field and associated histogram for case 3.

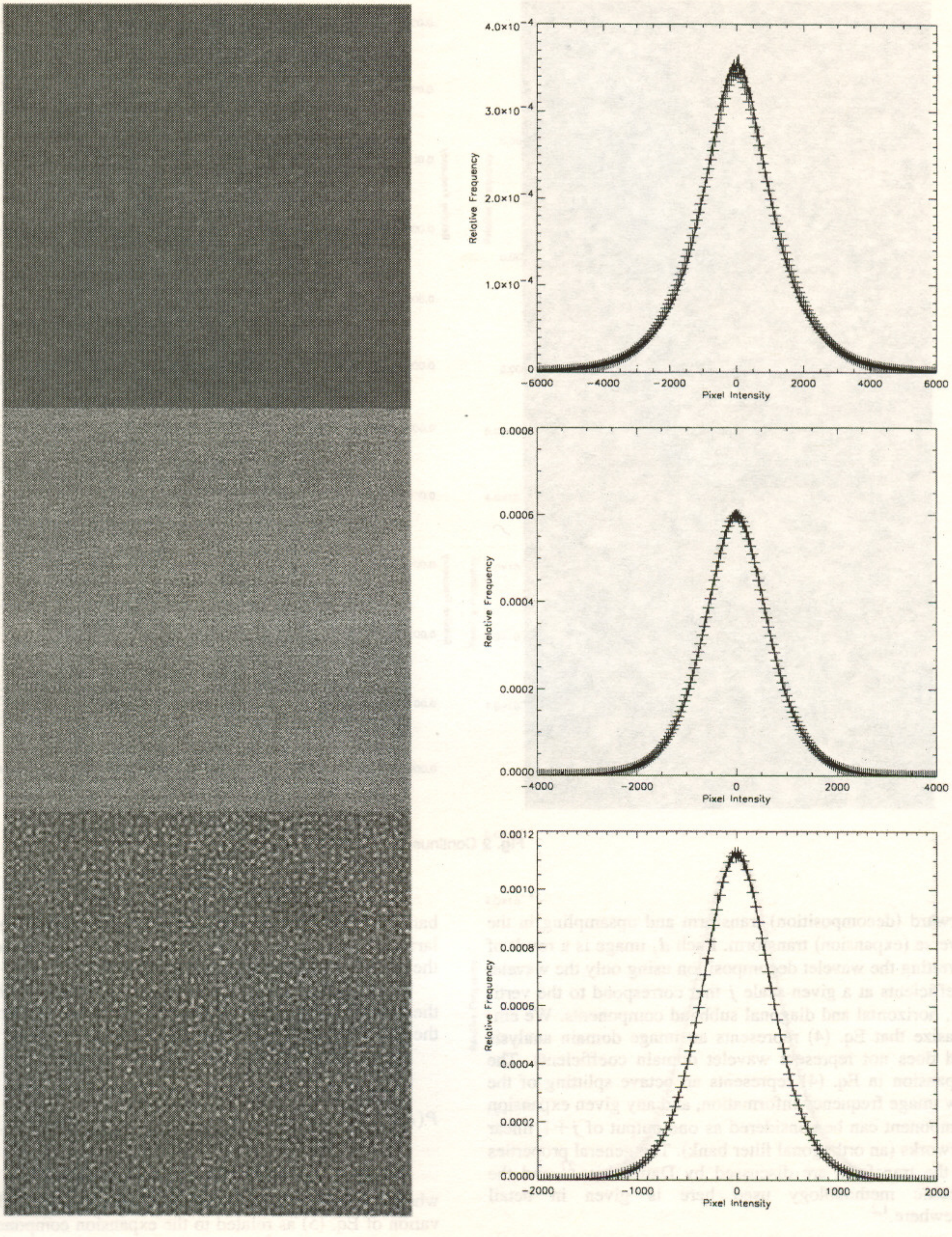

Fig. 2 Case 1: expansion components d_1 to d_5, top to bottom (left), respectively, and associated pdf modeling (right). The empirical histograms (solid) are to be compared to the theoretical (crosses) approximations. 512×512 pixel regions of interest are used for viewing purposes; although, all the data are used for the analysis. Points have been skipped on theoretical plots to avoid confusion.

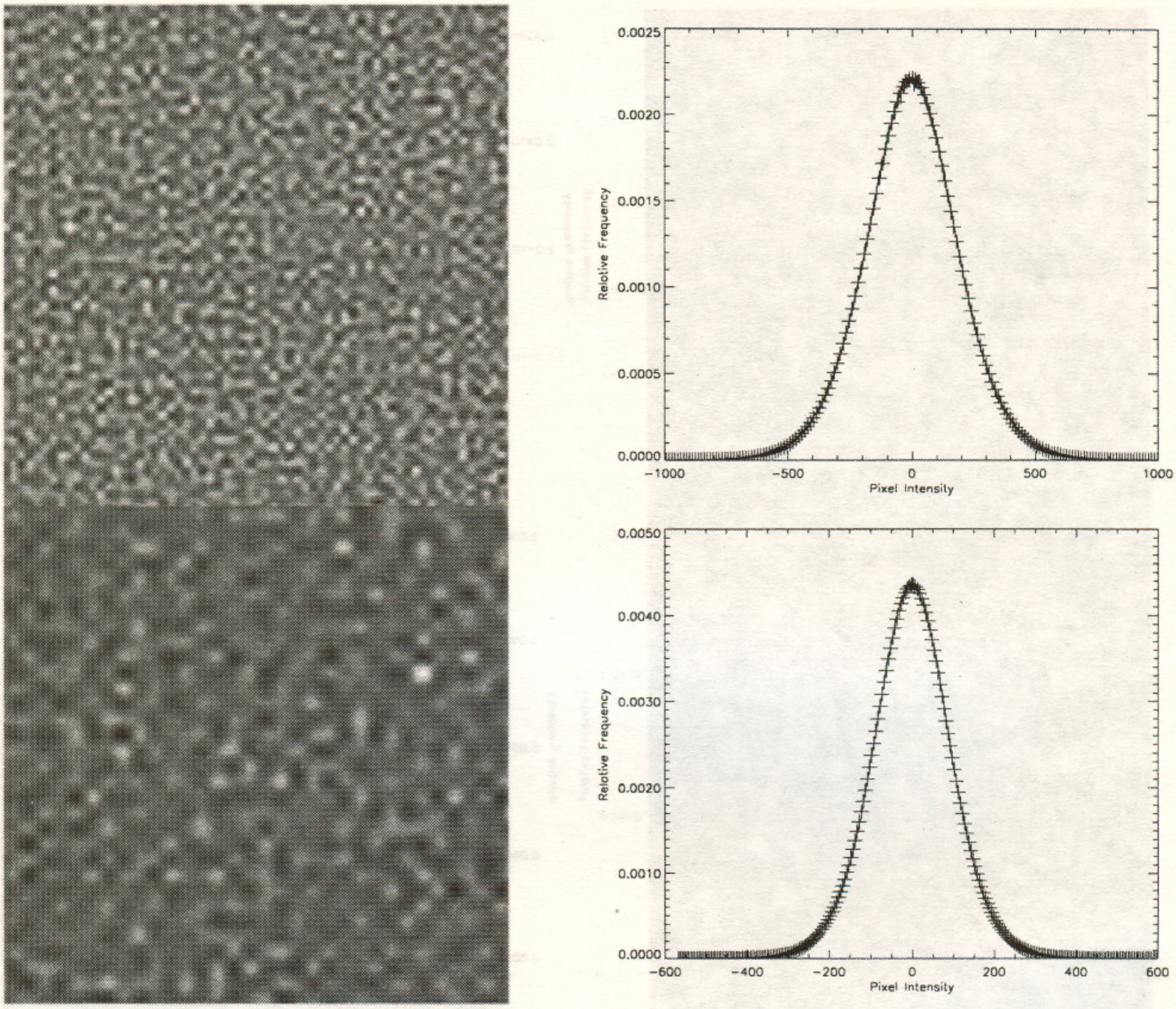

Fig. 2 Continued.

forward (decomposition) transform and upsampling in the inverse (expansion) transform. Each d_j image is a result of inverting the wavelet decomposition using only the wavelet coefficients at a given scale j that correspond to the vertical, horizontal and diagonal subband components. We emphasize that Eq. (4) represents an image domain analysis and does not represent wavelet domain coefficients. The expansion in Eq. (4) represents an octave splitting of the raw image frequency information, and any given expansion component can be considered as one output of $j+1$ linear networks (an orthogonal filter bank). The general properties of the transform are discussed by Daubechies,[27] and the specific methodology used here is given in detail elsewhere.[1,2]

4 Random Field Analysis

The three cases and associated empirical histograms are shown in Figs. 1(a) to 1(c), respectively. It is interesting to note that for case 3, a seemingly irregular multimodal field is derived from a simple linear transformation of a wide-band process (that is, from case 1). There are striking similarities with mammographic images in appearance and with the irregular histogram for case 3.

The general characteristic function associated with both the wavelet expansion component probability modeling and the input field distribution is given by

$$P(\omega)=\frac{k^{2\gamma}}{(k^2+\omega^2)^\gamma}, \tag{5}$$

where k and γ are positive parameters. A theoretical derivation of Eq. (5) as related to the expansion components is provided elsewhere.[3] For the special case, $\gamma=N$, the inverse FT of (5) gives the desired pdf expression

$$p(z)=\frac{k\exp(-k|z|)}{2^{2N-1}(N-1)!}\sum_{l=0}^{N-1}\frac{(2N-l-2)!(2|z|k)^l}{l!(N-l-1)!}, \tag{6}$$

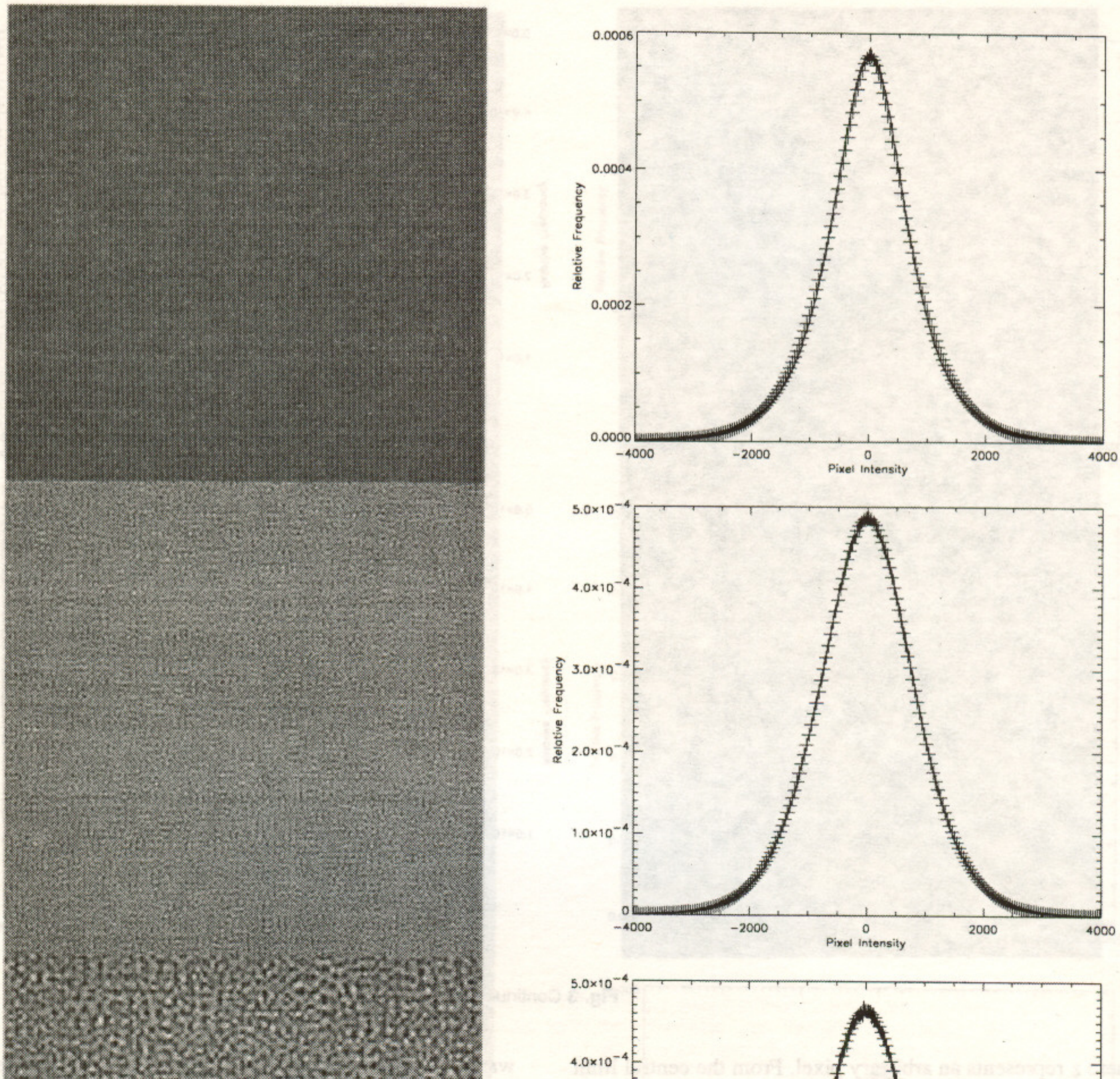

Fig. 3 Case 2: $\beta=1$ expansion components d_1 to d_5, top to bottom (left), respectively, and associated pdf modeling (right). The empirical histograms (solid) are to be compared to the theoretical (crosses) approximations. 512×512 pixel regions of interest are used for viewing purposes; although, all the data are used for the analysis. Points have been skipped on theoretical plots to avoid confusion.

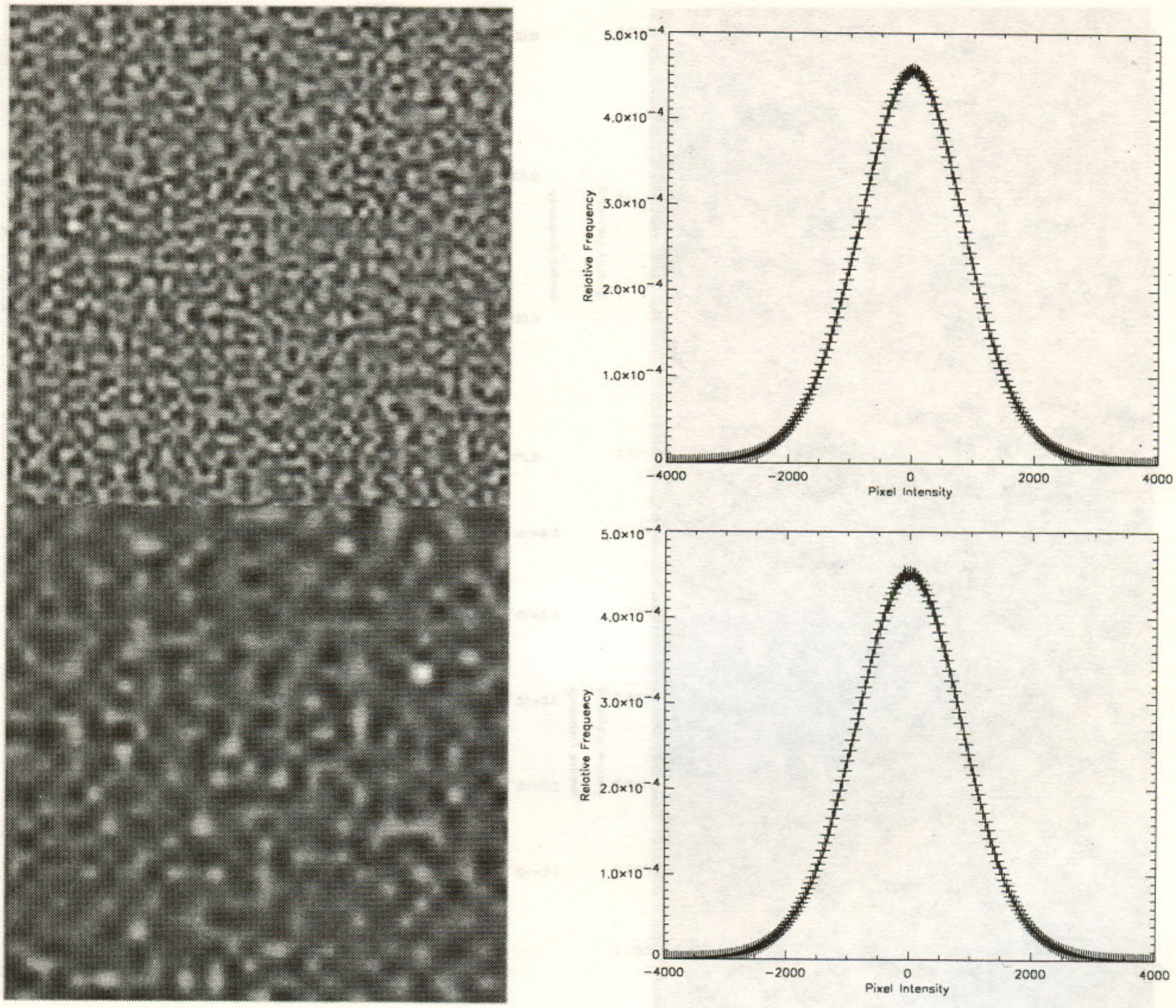

Fig. 3 Continued.

where z represents an arbitrary pixel. From the central limit theorem, Eq. (6) approaches a normal distribution for large N.

Random fields described by Eq. (6) can be generated from the RV transformation

$$Z=\sum_{i=1}^{2N} X_i^2-Y_i^2, \tag{7}$$

where X_i and Y_i are identically distributed, independent, zero mean Gaussian RVs. This is recognized as adding N Laplace distributed RVs.[28] The k_0 process results from lifting the integer N restriction and letting $N=1/2$ in Eq. (7). It is important to note that this is not represented by Eq. (6). Likewise, the k_0 pdf is derived by letting $\gamma=1/2$ in Eq. (5) followed by Fourier inversion. Gaussian RVs used in Eq. (7) are generated with the Box-Mueller method starting with uniformly distributed RVs.[29]

Our interest in fields distributed as Eq. (6) is a result of previous mammographic image analysis. This form was first used as an approximation for the mammographic wavelet expansion component modeling. Subsequent research,[4] that involved solving Eq. (1) for $s(x,y)$ for actual mammograms by making reasonable estimates of $H(f)$, resulted in fields that can be reasonably well approximated by Eqs. (5) and (6). Other researchers have studied the multiresolution properties of 2-D $1/f$ fields[12,30] by analyzing the wavelet coefficient properties (or decimated filter outputs). Our work is different in that we analyze the expansion components.

The expansion in Eq. (4) is carried out for $J=5$, for each simulation case. Figure 2 shows modeling for the case 1 field for the d_1 through d_5 images (top to bottom), where the corresponding N values are 2, 3, 4, 5, and 6, respectively. The case 2 expansion is shown in Fig. 3 with the corresponding N values given by 2, 4, 6, 8, and 10. For case 3, shown in Fig. 4, the corresponding N values are 2, 5, 7, 8, and 10. Generally for this study, we are interested in the form of the expansion component (choosing the proper N) and not the scaling parameter, k, in Eq. (6). Therefore, we have not provided these values. Standard regression meth-

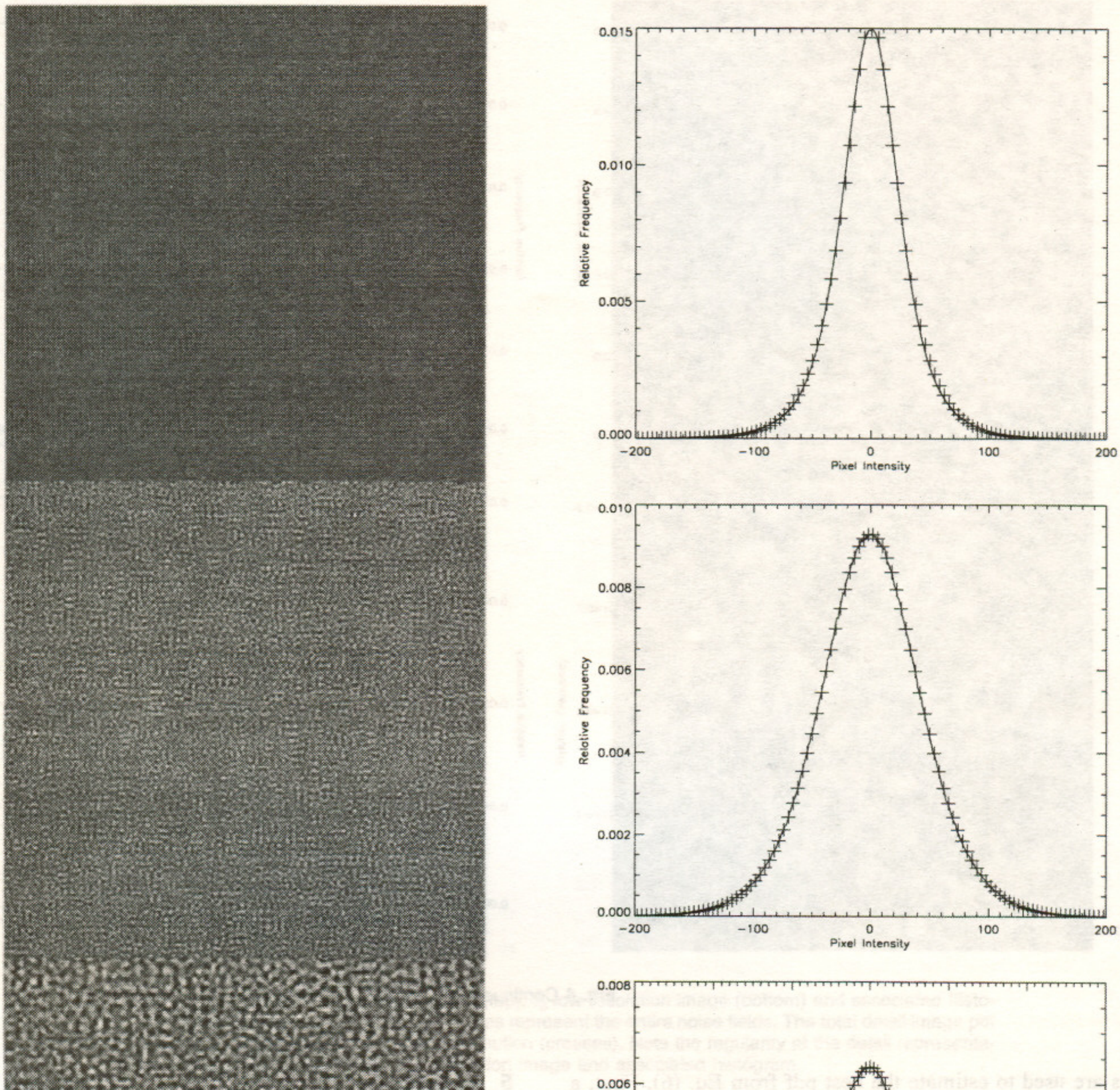

Fig. 4 Case 3: $\beta=1.5$ expansion components d_1 to d_5, top to bottom (left) respectively, and associated pdf modeling (right). The empirical histograms (solid) are to be compared to the theoretical (crosses) approximations. 512×512 pixel regions of interest are used for viewing purposes, although all the data are used for the analysis. Points have been skipped on theoretical plots to avoid confusion.

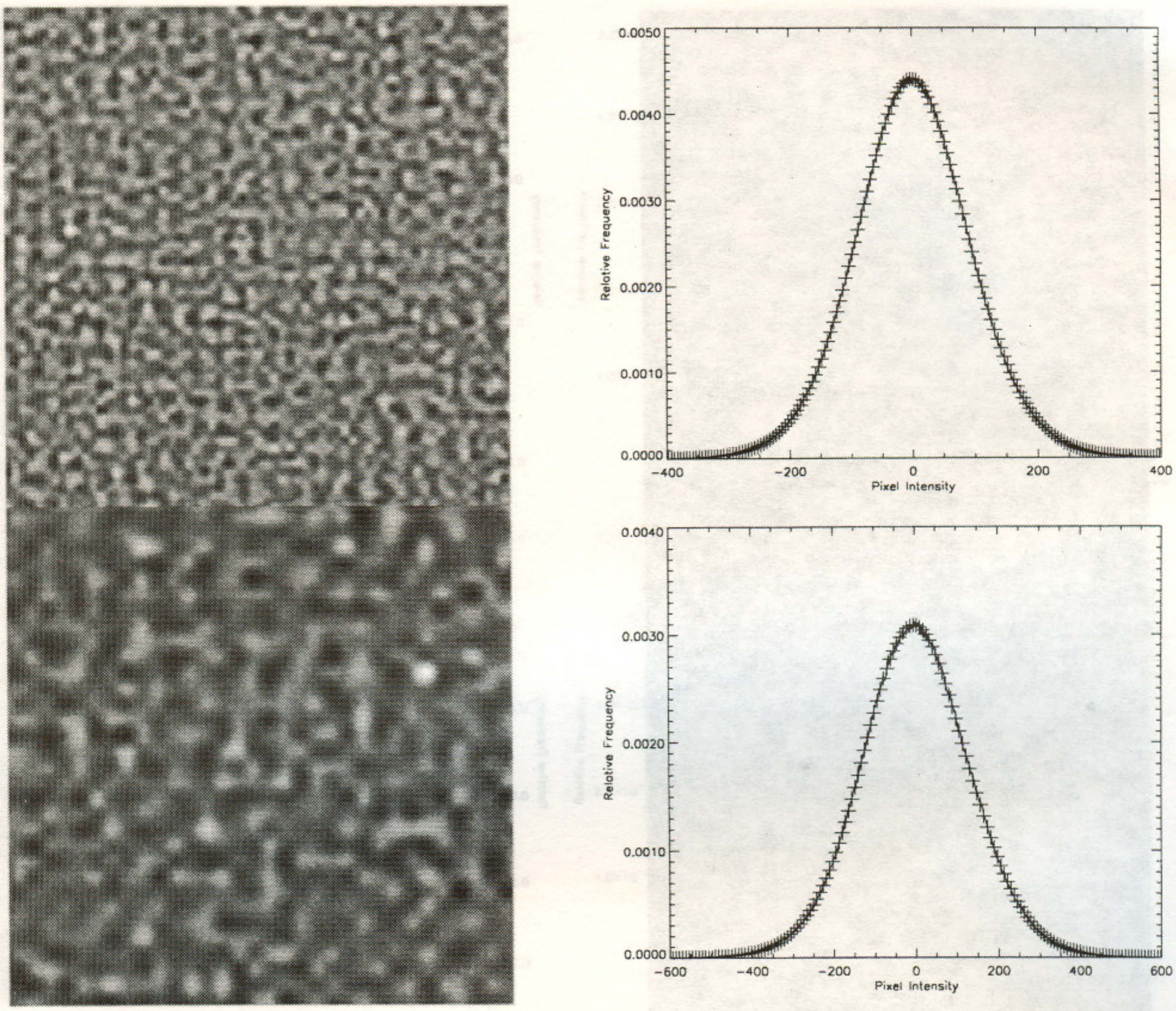

Fig. 4 Continued.

ods are used to estimate the best pdf from Eq. (6). First, a number of pdfs for different N values (1 to 15) are fit with the standard least squares methods to a given expansion component. Then, all of the theoretical pdfs are compared with the data; the curve that best agrees with the data is used as the model. The three important inferences are: (I) the approximations appear reasonable and (II) the expansion components can be regular even though the process behaves in an irregular fashion. This can be demonstrated by combining the detail images for case 3, shown in Fig. 5 (top). To a good approximation the component modeling is Gaussian. Figure 5 (bottom) shows the f_5 image [see Eq. (4)] and associated empirical histogram. Note that many of the irregularities are very similar to the case 3 image; and most importantly, (III) case 3 shows signs of irregular behavior, note the multimodal appearance of the histogram. Note that mammograms also behave in this fashion. This agrees with the development provided in the Appendix, which shows the process is not well defined for $\beta \geqslant 1.5$. By comparison, this behavior is not exhibited as much for case 2 because it is within the permitted β values.

5 Discussion

An approximation method was used to model the expansion components of a multiresolution wavelet analysis for the fields studied for a particular wavelet basis. We have not addressed the relationship with the probability modeling and the wavelet basis. Since there are many different bases and each wavelet basis has different frequency characteristics, it is safe to assume that the probability modeling would change when changing basis, and there is evidence that this is the case.[31] In general, we found that using a basis with fewer coefficients results in a decreased N value for a given expansion component. We qualify this with the understanding that we have not completed a thorough investigation with a large number of wavelet bases, and this does not agree for the Haar basis, where contrary behavior is observed. This also indicates that better approximations can be found by lifting the restriction on γ, although the pdf modeling becomes more complex. Strictly, the analysis applies to fields that have random phases derived from driving white noise through some linear network. Preliminary

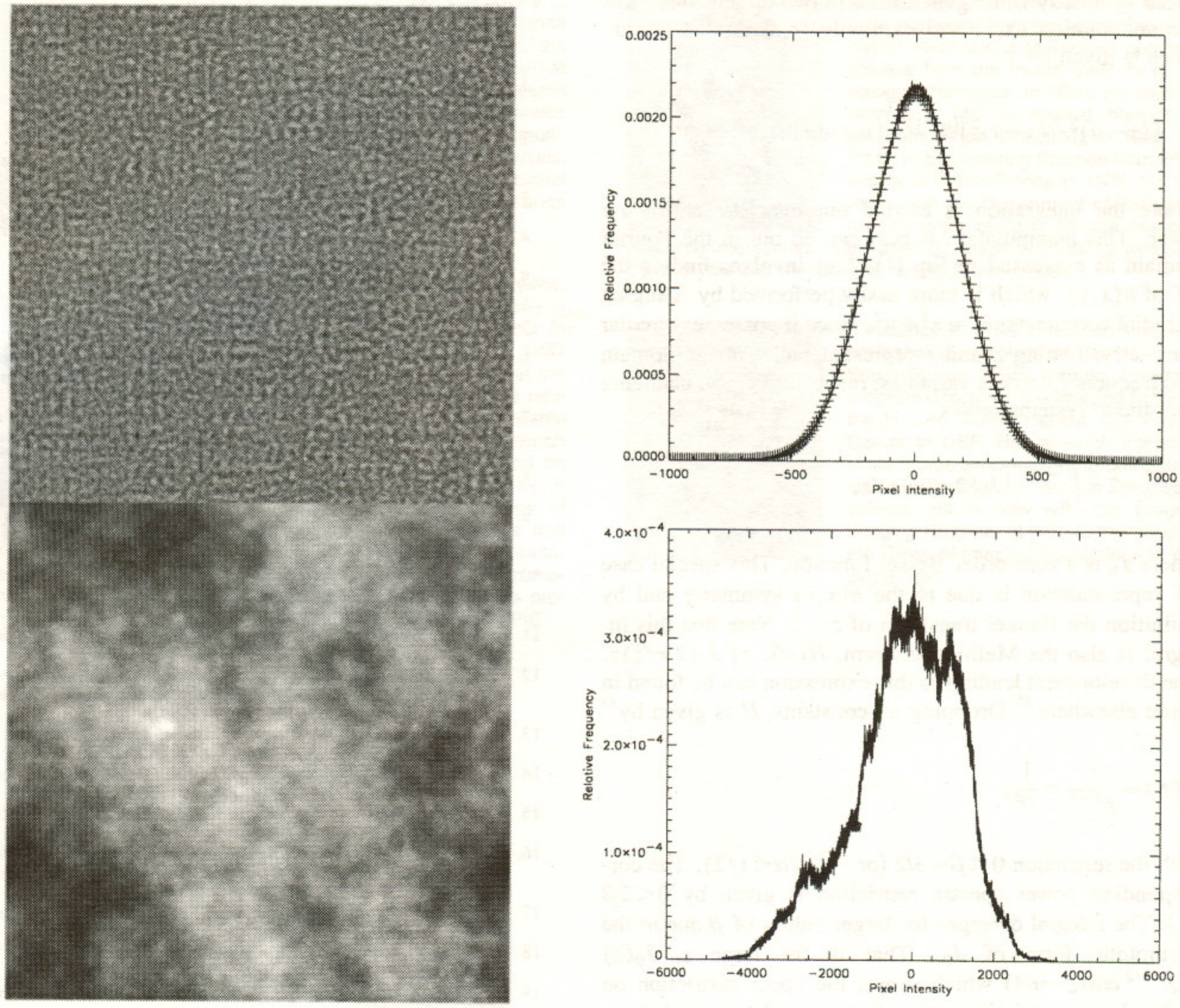

Fig. 5 Addition of the five detail images (top), f_5 low resolution image (bottom) and associated histograms for the third case (Fig. 4). The figures represent the entire noise fields. The total detail image pdf (solid) is approximated as a normal distribution (crosses). Note the regularity of the detail representation and the irregularity of the low resolution image and associated histogram.

evidence indicates that the random phase model applies to mammographic images.[4]

This research shows that to understand the multiresolution statistical nature of certain $1/f$ processes it is beneficial to consider the process as resulting from driving noise through a suitable filter, and analyze the probability character of the noise by solving Eq. (1). This work provides evidence that when fields distributed as Eq. (5) or Eq. (6) undergo certain linear transforms, such as the $1/f$ filtering, the resulting multiresolution expansion fields are distributed (approximately) similarly with different parameters. This comes from considering the possibility of changing the order of the two linear operations discussed here, for example: (a) apply the wavelet expansion to the raw field for case 1 and (b) then apply the $1/f$ filtering to each individual expansion component, which is the reverse order of the analysis shown here but is equivalent.

It would be a bit optimistic to imply that Eq. (5) is universal for all gray scaled images. Future work will include similar analysis for input fields distributed with other pdfs and theoretical approximations based on a linear operator formalism.[3]

6 Appendix

Equation (1) can be expressed in the image domain as the 2-D convolution

$$h(x,y)**s(x,y).$$

By generalizing the previous one dimensional work,[17,24,25] the filter $h(x,y)$ given by

$$h(x,y)=(x^2+y^2)^{(\alpha-1)/2},$$

where normalization factors have been dropped. We have forced symmetry by assuming the original 1-D form gives radial symmetry when generalized in two dimensions. Now the convolution expressed explicitly in Cartesian coordinates is given by

$$\int_{u,t} [(x-u)^2+(y-t)^2]^{(\alpha-1)/2} s(u,t)\,du\,dt,$$

where the integration is carried out over the entire u-t plane. This manipulation is best carried out in the Fourier domain as expressed in Eq. (1). This involves finding the FT of $h(x,y)$, which is more easily performed by changing to radial coordinates $z^2=x^2+y^2$, since it possesses circular symmetry. Letting z and f represent radial image domain and frequency domain variables, respectively, and changing coordinate systems, gives

$$H(f)=2\pi\int_0^\infty z^{\alpha-1} J_0(2\pi f z) z\,dz,$$

where J_0 is a zero-order Bessel function. This special case FT representation is due to the $h(x,y)$ symmetry and by definition the Hankel transform of $z^{\alpha-1}$. Note that this integral is also the Mellin transform, $H(\alpha)$, of $J_0(2\pi f z)z$. The development leading to this expression can be found in detail elsewhere.[32] Dropping all constants, H is given by[33]

$$H(f)\approx\frac{1}{f^{\alpha+1}}=\frac{1}{f^{\beta}},$$

with the restriction $0<\beta<3/2$ (or $-1<\alpha<1/2$). The corresponding power spectra restriction is given by $0<2\beta<3$. The integral diverges for larger values of β due to the asymptotic form of J_0. That is for large z, $J_0(z)\approx z^{-1/2}\cos(z-\pi/4)$ which shows the upper restriction on α. The lower restriction comes from considering the behavior of the integral near $z=0$. That is with $\alpha=-1$, the integral behaves as $\int 1/z\,dz$ which has a logarithmic singularity at $z=0$, but this is not a problem since $\alpha=-1$ is excluded in the interval $-1<\alpha<1/2$. For our considerations, it is the upper α region that is important because to a good approximation mammograms fall in this outer range for many cases in our database. As in the simulation, with $\beta=1.5$, the resulting output from the filtering operation becomes unstable. It is for this reason the cases 2 and 3 simulations exhibit much different behavior. Although in practice, this does not appear to be a hard limit. The irregular multimodal histogram characteristic begins to develop somewhere in between the case 1 and case 2 simulations. It is also interesting to note that repeating the experiment with different realizations of a given $s(x,y)$ field for $\beta=1.5$ results in output fields with empirical histograms that differ significantly, and for all practical purposes are not different realizations of the same process.

Acknowledgment

The authors would like to thank Prof. Ismail A. Sakmar for his mathematical insight that enhanced the manuscript.

References

1. J. J. Heine, S. R. Deans, D. K. Cullers, R. Stauduhar, and L. P. Clarke, "Multiresolution statistical analysis of high-resolution digital mammograms," *IEEE Trans. Med. Imaging* **16**, 503–515 (1997).
2. J. J. Heine, S. R. Deans, D. K. Cullers, R. Stauduhar, and L. P. Clarke, "Multiresolution resolution probability analysis of gray scaled images," *J. Opt. Soc. Am. A* **15**, 1048–1058 (1998).
3. J. J. Heine, S. R. Deans, and L. P. Clarke, "Multiresolution probability analysis of random fields," *J. Opt. Soc. Am. A* **16**, 6–16 (1999).
4. J. J. Heine, S. R. Deans, R. P. Velthuizen, and L. P. Clarke, "On the statistical nature of mammograms," *Med. Phys.* (in press).
5. C. E. Priebe, J. L. Solka, R. A. Lorey, G. W. Rogers, W. L. Poston, M. Kallergi, W. Qian, L. P. Clarke, and R. A. Clark, "The application of fractal analysis to mammographic tissue classification," *Cancer Lett. (Shannon, Ireland)* **77**, 183–189 (1994).
6. F. Lefebvre, H. Benali, R. Gilles, E. Kahn, and R. Di Paola, "A fractal approach to the segmentation of microcalcifications in digital mammograms," *Med. Phys.* **22**, 381–390 (1995).
7. V. Velanovich, "Fractal analysis of mammographic lesions: a feasibility study quantifying the difference between benign and malignant masses," *Am. J. Med. Sci.* **311**, 211–214 (1996).
8. A. P. Pentland, "Fractal-based description of natural scenes," *IEEE Trans. Pattern. Anal. Mach. Intell.* **6**, 661–674 (1984).
9. D. J. Field, "Relations between the statistics of natural images and the response properties of cortical cells," *J. Opt. Soc. Am. A* **4**, 2379–2394 (1987).
10. J. Huang and D. L. Turcotte, "Fractal image analysis: application to the topography of Oregon and synthetic images," *J. Opt. Soc. Am. A* **7**, 1124–1130 (1990).
11. T. Peli, "Multiscale fractal theory and object characterization," *J. Opt. Soc. Am. A* **7**, 1101–1112 (1990).
12. G. H. Watson and S. K. Watson, "Detection of unusual events in intermittent non-Gaussian images using muliresolution background models," *Opt. Eng.* **35**, 3159–3171 (1996).
13. D. L. Ruderman and W. Bialek, "Statistics of natural images: scaling in the woods," *Phys. Rev. Lett.* **73**, 814–817 (1994).
14. P. Caligiuri, M. L. Giger, and M. Favus, "Multifractal radiographic analysis of osteoporosis," *Med. Phys.* **21**, 503–508 (1994).
15. J. C. Hart, "Fractal image compression and recurrent iterated function systems," *IEEE Comput. Graph. Appl.* **16**, 25–33 (July 1996).
16. F. Espinal, T. Huntsberger, B. D. Jawerth, and T. Kubota, "Wavelet-based fractal signature analysis for automatic target recognition," *Opt. Eng.* **37**, 166–174 (1998).
17. G. Wornell, *Signal Processing with Fractals: A Wavelet-Based Approach*, Prentice Hall, England Cliffs (1996).
18. P. Kube and A. Pentland, "On the imaging of fractal surfaces," *IEEE Trans. Pattern. Anal. Mach. Intell.* **10**, 704–707 (1988).
19. J. Theiler, "Estimating fractal dimension," *J. Opt. Soc. Am. A* **7**, 1055–1073 (1990).
20. Q. Huang, J. R. Lorch, and R. C. Dubes, "Can the fractal dimension of images be measured?," *Pattern Recogn.* **27**, 339–349 (1994).
21. J. F. Veenland, J. L. Grashuis, F. Van der Meer, A. L. D. Beckers, and E. S. Gelsema, "Estimation of fractal dimension in radiographs," *Med. Phys.* **23**, 585–594 (1996).
22. B. Gold and G. O. Young, "The response of linear systems to non-Gaussian noise," *IRE Trans. Inf. Theory* **PGIT 2-4** 63–67 (1953/54).
23. G. Arfken, *Mathematical Methods for Physicists*, 2nd ed., Academic Press, New York (1970).
24. J. A. Barnes and D. W. Allan, "A statistical model of flicker noise," *Proc. IEEE* **54**, 176–178 (1966).
25. K. B. Oldham and J. Spanier, *The Fractional Calculus*, Academic Press, New York (1974).
26. L. Andersson, N. Hall, B. Jawerth, and G. Peters, "Wavelets on closed subsets of the real line," in *Recent Advances in Wavelet Analysis*, L. L. Schumaker and G. Webb, Eds., Academic Press, Boston (1994).
27. I. Daubechies, *Ten Lectures on Wavelets*, Society for Industrial and Applied Mathematics, Philadelphia (1992).
28. N. L. Johnson, S. Kotz, N. Balakrishnan, *Continuous Univariate Distributions, Vol. 2*, 2nd ed., Wiley, New York (1995).
29. W. H. Press, S. A. Teukolsky, W. T. Vetterling, and B. P. Flannery, *Numerical Recipes in C. The Art of Scientific Computing*, 2nd ed., Cambridge University Press, New York (1992).
30. J. G. Jones, R. W. Thomas, P. G. Earwicker, and S. Addison, "Multiresolution statistical analysis of computer-generated fractal imagery," *CVGIP: Graph. Models Image Process.* **53**, 349–363 (1991).
31. J. J. Heine, "Multiresolution statistical analysis of high resolution digitized mammograms and other gray scaled images," PhD Dissertation, Univ. of South Florida (Dec. 1996).
32. R. N. Bracewell, *Two-Dimensional Imaging*, Prentice-Hall, Englewood Cliffs, NJ (1995).
33. I. S. Gradshteyn, I. M. Ryzhik, *Tables of Integrals, Series, and Products*, 5th ed., p. 707, Academic Press, Boston (1994).

John J. Heine is an assistant professor of radiology at the University of South Florida (USF), Tampa, Florida, and member of the Digital Medical Imaging Program (DMIP) at the H. Lee Moffitt Cancer and Research Center at USF. Current research interests include random variable analysis, multiresolution analysis, fractal image analysis, and Fourier methods as applied to digital mammography and magnetic resonance imaging.

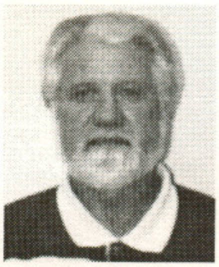

Stanley R. Deans is professor of physics, and jointly in radiology, at the University of Sough Florida. He received his PhD in physics at Vanderbilt University in 1967 and has been a postdoctoral fellow at the University of California, Berkeley. He held a National Research Council Associateship for three years at NASA Ames Research Center in California where he worked on problems of detection of weak signals in noisy ensembles. Dr. Deans is author of the book *The Radon Transform and Some of Its Applications*, and he has written several articles and reviews of Radon and Abel transforms. He also has research and writing interests in quantum mechanics, wavelet transforms, and computational methods. His professional affiliations include APS, AAPM, IEEE, SIAM, and SPIE.

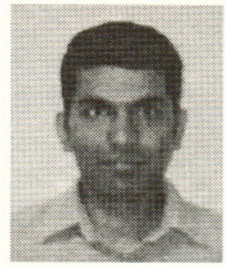

Deepak Gangadharan received a BSc degree in physics from the University of Bombay in 1986 and a M Tech in engineering physics from the Indian Institute of Technology, Kharagpur, in 1990. He went on to receive a MS in applied physics from Northern Illinois University in 1994 and a Ph.D. in Engineering Science from the University of South Florida in 1998. He is currently with the Department of Radiology at the University of South Florida. His current research interests include wavelets, image processing, and statistical analysis and modeling of radiographic images.

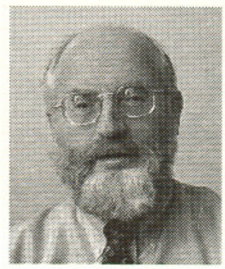

Laurence P. Clarke was, until recently, a professor of radiology at the University of South Florida (USF), Tampa, Florida, and program director of the Imaging Program at the H. Lee Moffitt Cancer and Research Center at USF. His research interests include image processing and computed assisted diagnosis for various imaging modalities. He is now with the Diagnostic Imaging Program at NCI as branch chief of the Office of Imaging Technology in Washington, DC.